Journal of the European Ceramic Society 17 (1997) 697–711

PII: S0955-2219(96)00090-8
0955-2219/97/$17.00

Characterization of Die-Pressed Green Compacts

Necati Özkan & Brian J. Briscoe*

Department of Chemical Engineering and Chemical Technology, Imperial College of Science, Technology and Medicine, London SW7 2BY, UK

(Received 15 February 1996; revised version received 9 April 1996; accepted 3 May 1996)

Abstract

Die-pressed agglomerated alumina compacts, prepared as cylinders using single-ended nominally uniaxial compressive stresses, have been characterized by measuring their strength and density distributions. The strength of the alumina compacts, measured using the Brazilian configuration, increases up to an optimum compaction pressure; upon further increasing the compaction pressure, the strength of the green compacts decreases due to the formation of internal cracks. The density distributions in the alumina compacts have also been determined experimentally, using the coloured layer technique and also deduced indirectly from hardness measurements. The results obtained from these two experiments are shown to be in good agreement. The densest parts of the compacts, compressed uniaxially from the top planar surface adjacent to the compression source, are at the outer circumference at the top and the least dense parts are at the outer circumference at the bottom face. The density near the cylindrical surface of the compacts decreases with height from the top to the bottom of the compact. The density difference between the most dense and the least dense parts of the compacts increases with increasing aspect ratio; that is, the height-to-diameter ratio. The density distributions in the alumina compacts have also been estimated using a first-order predictive model. According to this model, the mean density variation along the height of the compact decreases linearly with height from the top to the bottom of the compact. These predictions are shown to be almost in accord with experiment. © 1997 Elsevier Science Limited. All rights reserved.

1 Introduction

The creation of an inhomogeneous stress distribution within a compact is an inherent problem in the application of the die-pressing technique using nominally dry powders. The case of single-ended nominal uniaxial compaction using planar platens within a cylindrical die provides a convenient example of this phenomenon in a simple but widely used compaction geometry. A nominal uniaxial pressure applied from the one end of the die, containing the powder, will be dissipated by the wall and internal friction so that a substantial portion of the powder will experience a much lower compressive pressure than the applied pressure. Naturally, these areas will compact to a lower density than those areas exposed to a higher pressure. As a result, a variable density distribution is created within the compacts due to these frictional effects. In practice, the use of suitable binders and wall lubricants can reduce both the wall and the particle friction and thus reduce the density variations in the green compacts.

In this paper, the pressure transmission process and its influence on the density variation during the compaction process for various types of agglomerates are reported. Two binder systems have been studied at a range of ultimate compaction pressures. The density distributions within the alumina compacts were measured experimentally using the coloured layer technique and inferred using hardness measurements. The density distributions of the compacts, as a function of the height of the compacts, are predicted using a first-order model and the predicted results are then compared with the experimental results.

Selected data are provided to relate the green strength to the compaction pressure. It is observed that there is an optimal compaction pressure for the production of the strongest green compact.

2 Materials and Experimental Procedure

2.1. Die-pressing

Various types of alumina agglomerates, prepared by spray drying and solution techniques, were used in this study to produce green compacts using the dry die-pressing technique. The preparation

*To whom correspondence should be addressed.

Table 1. Properties of the alumina agglomerates used in this work

Agglomerate ID[a]	*Agglomerate size (μm)*[b]	*Binder type & content (wt%)*[c]	*Moisture level (% H_2O)*[d]	*Preparation technique*
A/4/V/D	53–212	PVA, 4·70	Dry (0·0)	Solution
A/4/V/W	53–212	PVA, 4·70	Wet (1·2)	Solution
A/4/V/H	53–212	PVA, 4·70	Humid (0·35)	Solution
A/4/G/D	53–212	PEG, 4·70	Dry (0·0)	Solution
A/4/G/W	53–212	PEG, 4·70	Wet (1·3)	Solution
A/2/V/D	53–212	PVA, 2·40	Dry (0·0)	Solution
A/2/V/W	53–212	PVA, 2·40	Wet (1·2)	Solution
A/2/V/H	53–212	PVA, 2·40	Humid (0·3)	Solution
A/2/G/D	53–212	PEG, 2·40	Dry (0·0)	Solution
A/2/G/W	53–212	PEG, 2·40	Wet (1·1)	Solution
A/2/G/H	53–212	PEG, 2·40	Humid (0·3)	Solution
A/2·5/V/SD	53–212	PVA, 2·45	—	Spray dry
M/4/G/SD	~100	PEG, 4·10	—	Spray dry
M/4·5/G/SD	~100	PEG, 4·75	—	Spray dry

[a]Agglomerate identification: the agglomerates prepared using AKP-30 alumina (Sumitomo Ltd, Japan) with the mean particle size of 0·4 μm are denoted 'A' and M × 3 alumina (Morgan Matroc, UK) with the mean particle size of 1·2 μm are denoted 'M'.
[b]The size range of agglomerates.
[c]PVA, poly(vinyl alcohol); PEG poly(ethylene glycol).
[d]The 'dry' agglomerates were prepared by drying at 80°C in vacuum; the agglomerates with residual water which was not evaporated completely during agglomerate preparation are designated as 'wet'; the dry agglomerates which were conditioned in a vapour environment (saturated Na_2SO_3 solution) were designated as 'humid'.

procedure of these agglomerates is reported elsewhere.[1] The properties of these agglomerates are summarized in Table 1. The agglomerated powders were unidirectionally compacted in a 13 mm diameter cylindrical steel die. Compaction was achieved using a single-ended-acting plane punch operating against a fixed planar punch. The applied and transmitted pressures during the compaction process were measured simultaneously, using an apparatus attached to a commercial universal testing machine (Instron 1122, UK). A detailed description of this apparatus is given elsewhere.[2] Zinc stearate (BDH Chemicals, UK), a conventional solid lubricant, was used to lubricate the die walls.

2.2 Strength of green compacts

The diametrical compression test has been used to characterize the strength of the green compacts[3] (denoted later as fracture strength). The diametrical compression tests were carried out using the Instron universal testing machine. The loading platens, which were made from aluminium, were maintained parallel during the tests, and an aluminium foil was used as a 'padding material' in order to provide a more uniformly distributed load over the contact areas.

2.3 Density distribution measurements

The density distributions in powder compacts may be measured by a number of techniques. These techniques include: (i) the forming of identifiable layers of powder in the die;[4,5] (ii) the incorporation of materials opaque to X-rays whose migration during compaction may be followed by radiography, such as lead grids[6] and fine lead balls;[7] (iii) radiography including both X-rays[8] and gamma-rays;[9] and (iv) hardness measurements.[10,11]

The coloured layer technique, an example of category (i), and hardness measurements were used in the present study. Two batches of the M/4·5/G/SD agglomerates (see Table 1) with different colours (green and red) were produced by mixing the agglomerated powders with coloured solutions prepared from commercial inks dissolved in acetone. After removing the acetone from the mixture, the coloured M/4·5/G/SD agglomerates retained their good flow properties. In order to form the layers of different colours, the following procedure was applied. A quantity, 0·750 g, of coloured agglomerated powder was poured into the 13 mm steel die. The powder was pressed with an initial pressure of 0·74 MPa in order to provide sharp interfaces between the successive layers. The procedure was repeated using alternating colours until the desired number of layers was formed. The compacts were then formed at various ultimate compaction pressures. The axial cross-sections of the compacts were accessed by grinding with a silicon carbide abrasive paper. The thicknesses of the exposed coloured layers, as a function of the radius, were measured using a stereo microscope system with the associated accessories.[12]

The hardness measurements of the compacts were carried out using a standard universal testing machine (Instron 1122, UK) in conjunction with a hardened steel spherical indenter of radius 1·5 mm.

A separate linear variable displacement transducer was used to record the imposed displacement. The displacement may also be deduced from the crosshead approach velocity and lapsed time data. The indenter was fixed in a special holder fitted to the crosshead of the testing machine. The specimen was supported on the platform of the load cell. The hardness was computed following the procedures described in Section 3.3.2.

3 Experimental Results and Discussion

3.1 Strength of green compacts

The fracture strength of the green compacts was estimated using the diametrical compression test,[3] which is based on the state of stress developed when a cylindrical specimen is compressed between two diametrically opposite stress generators on its surface. For an ideal line-loading case, the maximum tensile stresses, which act across the plane containing the loading axis, have a constant magnitude which may be approximated by:

$$\sigma_M = \frac{2P}{\pi Dl} \quad (1)$$

where σ_M is the maximum tensile stress, P is the applied load at fracture, D is the diameter of the sample and l is the specimen length. The predicted form of the tensile fractures was invariably observed, and the typical types of fracture are illustrated in Fig. 1. When a centreline fracture occurred, the tests were considered valid (indicates of the sample strength).[3] The diametrical compression test results are summarized in Table 2. The computed green fracture strength of the M/4·5/G/SD compacts, as a function of the compaction pressure, is illustrated in Fig. 2. These data were obtained for a range of sample length l, but for a constant sample radius. As may be seen from Fig. 2, there is an optimum compaction pressure to achieve the highest possible fracture strength for these alumina compacts. The fracture strength of the green compacts increases up to the compaction pressure of ~370 MPa. Upon further increasing of the compaction pressure, the strength of the green compacts decreases due to the formation of laminar cracks. It is evident from Fig. 1 that the fracture characteristics of the compacts pressed at high pressures are different from those of the compacts pressed at compaction pressures of less than 370 MPa. Additional fractures (laminar cracks) occurred for the compacts pressed at high pressures.

It was also observed that there was a clear difference between the ejection force profiles (ejection force as a function of the imposed displacement) of the compacts pressed at high pressures and low pressures. Figures 3(a) and (b) illustrate the ejection profiles for the compacts pressed at 148 and 740 MPa, respectively. The ejection profile of the compact pressed at 740 MPa shows some irregularities (C1, C2 and C3) beyond point E (the point at which the compacts start to exit from the die). The positions of C1, C2 and C3 correspond to the locations of the laminar cracks which are apparent in this compact upon subsequent visual examination. No such discontinuities were apparent in the compact pressed at 148 MPa.

It may also be noted that the compacts produced from the agglomerates prepared using PVA as a binder are stronger than those produced from the agglomerates prepared using PEG as a binder.

3.2. Pressure transmission during compaction

During the compaction process, the applied compaction pressure will not be fully transmitted due to the dissipative frictional forces which exist between the particles and the die wall and between the particles themselves. The major source of the frictional forces is between the powder and the die wall. The level of the frictional forces depends upon the properties of the agglomerates, the aspect ratio and the surface condition of the die wall. In this section, the transmission ratios of the alumina compacts are reported and the effects of the aspect ratio, the state of wall lubrication and the agglomerate properties on the pressure transmission during the compaction process are described.

Figures 4(a), (b) and (c) shows curves of applied and transmitted pressures against displacement for the A/2·5/V/SD agglomerates with terminal H/D ratios of 0·526, 1·011 and 1·526, respectively. The difference between the applied and transmitted pressure curves for a low H/D ratio is small compared with the difference at larger H/D ratios. The effects of the aspect ratio on the transmission ratio can be seen clearly by plotting the ratio of the transmitted pressure to the applied pressure (transmission ratio) against the applied pressure. The plots of transmission ratio against the applied pressure for the alumina compacts are illustrated in Figs 5 and 6. The value of the stress transmission ratio increases as the compaction pressure is increased. The limiting pressure transmission ratio results (the asymptotic values at high compaction pressure) for the alumina compacts are summarized in Table 3.

The extent of the influence of friction between the powders and the die wall increases as the aspects ratio increases, and the pressure transmission ratio, as a consequence, decreases. Therefore, not only will the overall density of the compacts

decrease but also the density distribution will be more inhomogeneous. These experimental results will be used in a first-order model, to be described later, for the prediction of the general form of the green density distribution within the alumina compacts.

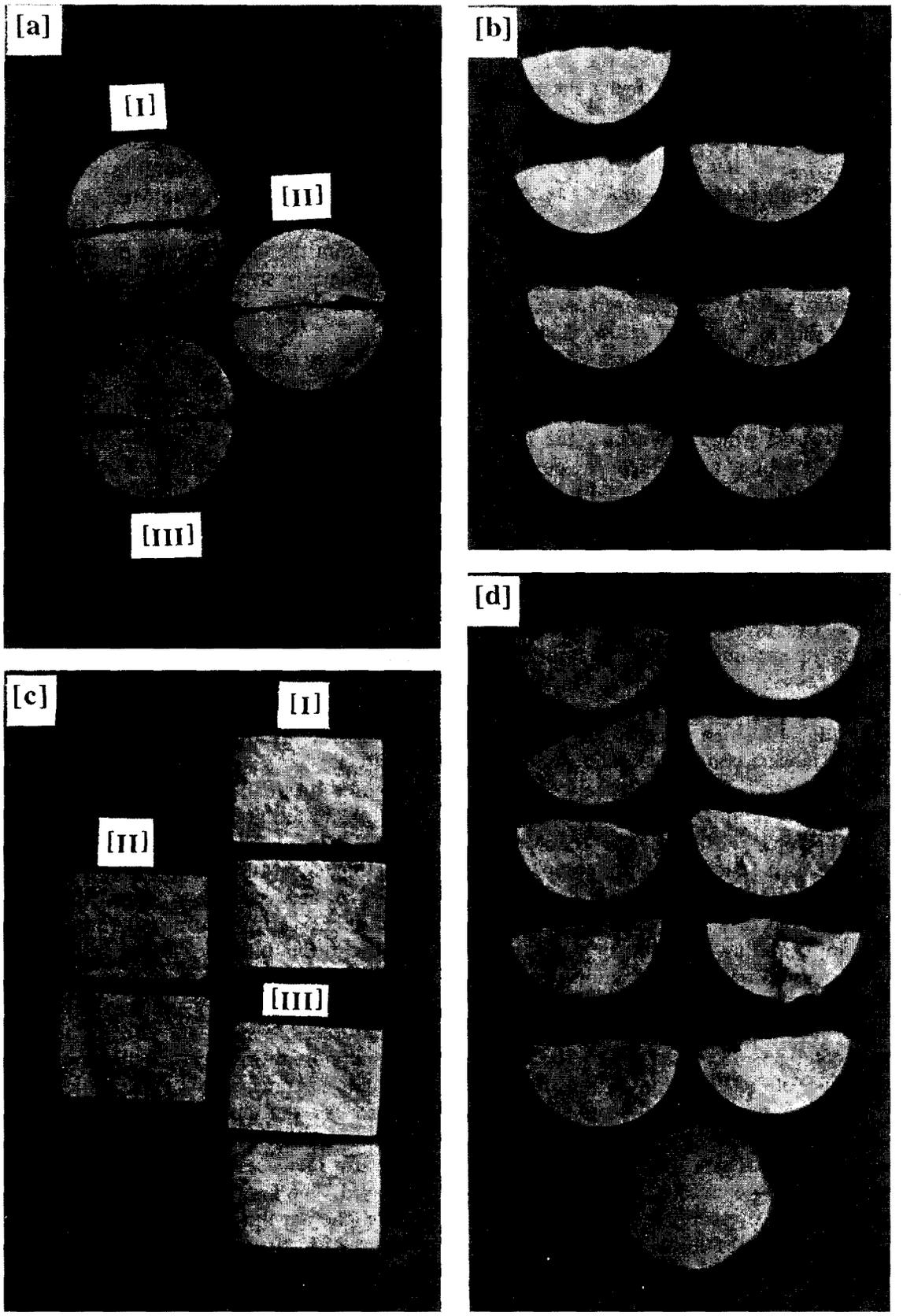

Fig. 1. Fracture characteristics of the alumina compacts during the diametrical compression test: (a) M/4·5/G/SD compacts (H/D = 0·70), pressed at [I] 74, [II] 148, and [III] 296 MPa; (b) M/4·5/G/SD compacts (H/D = 0·68), pressed at 740 MPa; (c) [I] A/2/V/H, [II] A/4/V/H and [III] A/2/G/H compacts with aspect ratio of ~0·97, pressed at 71 MPa; and (d) M/4·5/G/SD compact (H/D =1·15), pressed at 740 MPa.

Table 2. Green strength results for the alumina compacts

Compact[a]	*Compaction pressure (MPa)*[b]	H/D[c]	*Green density (%)*[d]	*Green strength (MPa)*[e]
M/4·5/G/SD	74	1·34	60·91	1·050
M/4·5/G/SD	74	0·73	61·12	0·996
M/4·5/G/SD	148	0·71	63·14	1·103
M/4·5/G/SD	222	0·70	64·22	1·156
M/4·5/G/SD	296	0·70	65·07	1·273
M/4·5/G/SD	370	0·70	65·77	1·474
M/4·5/G/SD	444	0·69	66·25	1·417
M/4·5/G/SD	518	0·69	66·70	1·111
M/4·5/G/SD	592	0·69	67·08	1·068
M/4·5/G/SD	740	0·68	67·73	1·015
M/4·5/G/SD	740	1·15	67·62	0·988
A/2/V/H (53 μm)	71	1·05	53·76	0·357
A/2/V/H (212 μm)	71	0·98	54·81	0·523
A/4/V/H (53 μm)	71	1·16	53·45	0·425
A/4/V/H (212 μm)	71	1·02	54·63	0·725
A/2/G/H (53 μm)	71	0·98	56·23	0·053
A/2/G/H (212 μm)	71	0·96	57·41	0·087
A/4/G/H (53 μm)	71	0·95	56·36	0·143
A/4/G/H (212 μm)	71	0·97	57·65	0·175

[a]The properties of the compacts are given in Table 1; for the agglomerates prepared using AKP-30 alumina (denoted as 'A'), two different agglomerate sizes were used.
[b]Ultimate applied compaction pressure.
[c]Aspect ratio (*H/D* = the height of the compact/the diameter of the compact) of the green compacts at the ultimate applied compaction pressure.
[d]Mean relative green density of the green compacts at the ultimate applied compaction pressure.
[e]Green strength of the green compacts calculated using eqn (1).

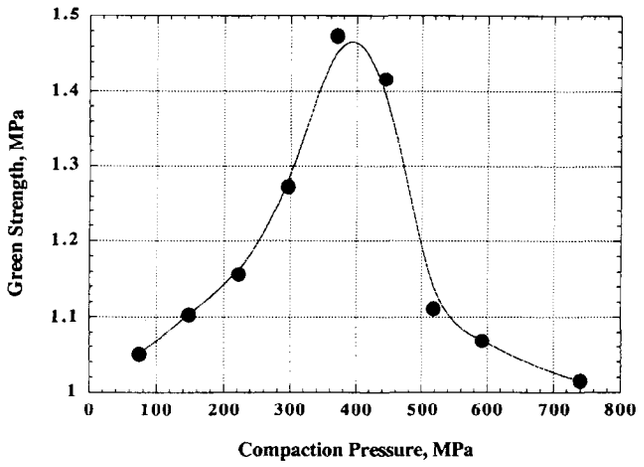

Fig. 2. Green strength of the M/4·5/G/SD alumina compacts as a function of compaction pressure.

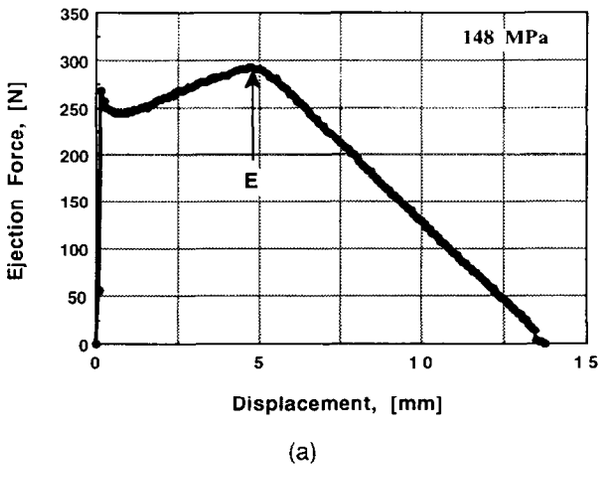

(a)

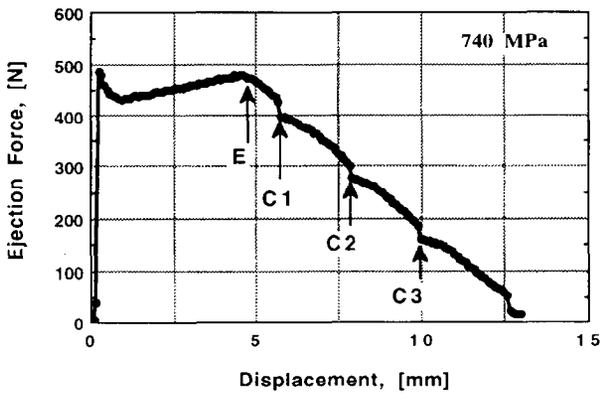

(b)

Fig. 3. Ejection profiles of the M/4·5/G/SD alumina compacts pressed at (a) 148 MPa and (b) 740 MPa.

3.3 Density distribution in alumina compacts

When a cylindrical powder compact is subjected to a load from the top of the die, the transmitted pressure decreases as the distance from the pressure source increases. Because the powder is confined in the die, the pressure is transmitted non-uniformly through the compact; that is, a complex and nonuniform stress distribution is created within the compact.

3.3.1 The coloured layer technique

Selected axial cross-sections of the compacts with the layers of alternating colours, used for the density distribution calculations, are shown in Fig. 7.

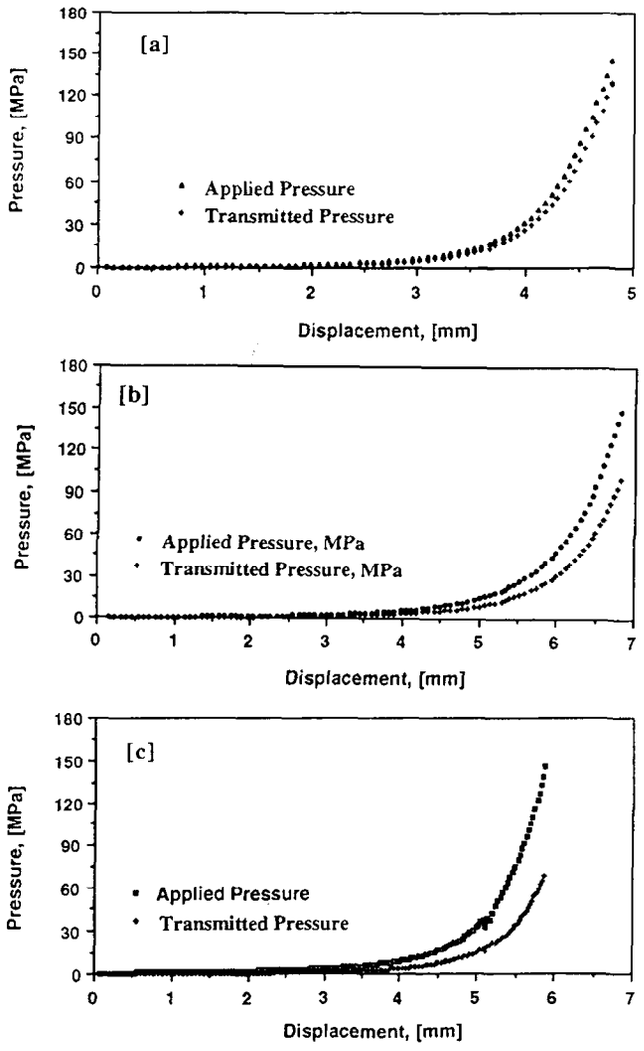

Fig. 4. Applied and transmitted pressures versus displacement curves for the A/2·5/V/SD compacts with the terminal aspect ratios of (a) 0·526, (b) 1·011 and (c) 1·526.

The properties of these compacts are summarized in Table 4. Because of the axial rotational symmetry, a single plane, placed across the diameter and in the axial direction, provides a complete description of the density distribution within the cylindrical compacts.

If the layers are compacted uniformly, the volumes of the layers V before and after the compaction, are given as follows:

$$V_0 = \pi r^2 h_0 \tag{2}$$

$$V_c = \pi r^2 h_c \tag{3}$$

The subscripts 0 and c denote the conditions prior to compaction and after compaction, respectively. Since the weight W, of the layers before and after compaction is the same, the density of the layers before and after the compaction will be given as:

$$\rho_0 = W/\pi r^2 h_0 \tag{4}$$

and

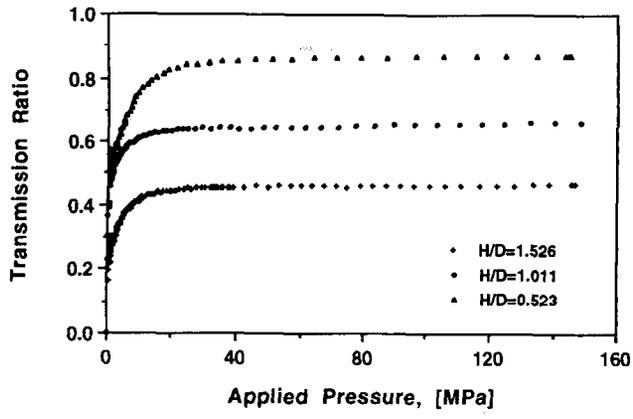

Fig. 5. Transmission ratio versus applied pressure curves for the A/2·5/V/SD compacts with the terminal aspect ratios of 0·523, 1·011 and 1·526.

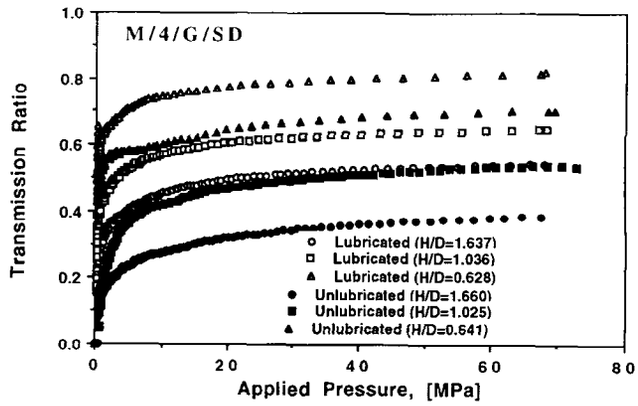

Fig. 6. Transmission ratio versus applied pressure curves for the M/4/G/SD compacts prepared in the lubricated (wall) and unlubricated dies.

$$\rho_c = W/\pi r^2 h_c \tag{5}$$

where r is the radius of the layer, h_0 is the height of the layer before compaction and h_c is the height of the layer after compaction. By rearranging eqns (4) and (5), we obtain:

$$h_0 = W/\pi r^2 \rho_0 \tag{6}$$

$$h_c = W/\pi r^2 \rho_c \tag{7}$$

where ρ_0 is the density before compaction and ρ_c is the density after compaction. Assuming that there is no significant radial movement of the powders during the compaction process, the density distribution at the curved lines of the demarcation planes may be calculated by measuring the strain in the axial direction, as a function of the radius, for the individual layers. By using eqns (6) and (7), we obtain the following interrelationship between strain and density:

$$\varepsilon_a = \frac{h_0 - h_c}{h_0} = \frac{\rho_c - \rho_0}{\rho_c} \tag{8}$$

where ε_a is the strain in the axial direction.

The computed density distributions along the curved demarcation lines, for the individual layers

Table 3. Experimental transmission ratios for the alumina compacts

Compacts[a]	*Compaction pressure (MPa)*[b]	*Aspect ratio*[c]	*State of lubrication*[d]	*Transmission ratio*[e]
A/2·5/V/SD	~145	0·526	Lubricated	0·86
A/2·5/V/SD	~145	1·011	Lubricated	0·69
A/2·5/V/SD	~145	1·526	Lubricated	0·47
A/2/V/D	~230	0·488	Lubricated	0·81
A/2/V/D	~230	0·960	Lubricated	0·68
A/2/V/D	~230	1·466	Lubricated	0·59
A/2/V/W	~230	0·478	Lubricated	0·84
A/2/V/W	~230	0·944	Lubricated	0·70
A/2/V/W	~230	1·390	Lubricated	0·63
A/2/G/W	~230	0·477	Lubricated	0·85
A/2/G/W	~230	0·957	Lubricated	0·72
A/2/G/W	~230	1·419	Lubricated	0·64
A/2/G/W	~230	0·491	Lubricated	0·82
A/2/G/W	~230	0·945	Lubricated	0·69
A/2/G/W	~230	1·397	Lubricated	0·62
M/4/G/SD	~70	0·628	Lubricated	0·82
M/4/G/SD	~70	1·036	Lubricated	0·65
M/4/G/SD	~70	1·637	Lubricated	0·54
M/4/G/SD	~70	0·641	Unlubricated	0·72
M/4/G/SD	~70	1·025	Unlubricated	0·53
M/4/G/SD	~70	1·660	Unlubricated	0·39
M/4·5/G/SD	222	0·506	Lubricated	0·87
M/4·5/G/SD	222	0·845	Lubricated	0·73
M/4·5/G/SD	222	1·536	Lubricated	0·49

[a]For the properties of the compacts see Table 1.
[b]Ultimate applied compaction pressure.
[c]Aspect ratio of the green compacts at the ultimate compaction pressure.
[d]The lubricated state was achieved by applying the zinc stearate powder to the die walls using a camelhair brush.
[e]Transmission ratio (the applied pressure/transmitted pressure) at the ultimate compaction pressure.

of the compacts, are illustrated in Fig. 8. The calculated highest density is at the top corners of the compacts and the lowest density is at the bottom corners. The density near the surface of the compacts decreases with height from the top to the bottom of the compact. In the axis of symmetry, the maximum density is observed in the lower half of the compact at a point close to the bottom of the compact, and the minimum density is observed at the top. The density distributions of the middle layers, in the diametrical direction, are relatively homogeneous.

The mean green densities of the individual layers of the compacts were calculated by measuring the total volume of each layer. In order to measure the volume of the layers, the height of the layers as a function of the distance from the centre of the compacts was measured using a microscope. By fitting a fifth-order polynomial curve to the measured height values, a function $f(r)$ representing the height of the layer was obtained. The volumes of the layers were then calculated using the following equation.[13]

$$V = 2\pi\int_0^r rf(r)\mathrm{d}r \tag{9}$$

where r is the radius of the compact. The volume of sections of the layers with radii ranging between r_1 and r_2 may also be calculated as:

$$V = 2\pi\int_{r_1}^{r_2} rf(r)\mathrm{d}r \tag{10}$$

The mean density of the layers and the mean density of the sections of the layers with 0·05 cm radius intervals were calculated using eqns (9) and (10), respectively (mean density = weight/volume). From the mean density of the sections of the layers, the approximate contours of equal density are then computed in order to obtain the density distribution patterns for the compacts.

The mean density of the layers together with the density distribution pattern for compacts A (lubricated, H/D = 1·537) and D (unlubricated, H/D = 1·552) are shown in Figs 9 and 10, respectively. For compact D, the highest mean density exists at the top layer. However, in the case of compact A, the mean density of the top layer is not of the highest density; rather it is at the third layer from the top.

3.3.2 Hardness measurements

The hardness of the compact at selected points was measured by using a spherical indenter with a radius of 1·5 mm. The expression adopted for approximation of the hardness H was:

$$H = \frac{P}{A} = \frac{P}{\pi(2Rh_p - h_p^2)} \tag{11}$$

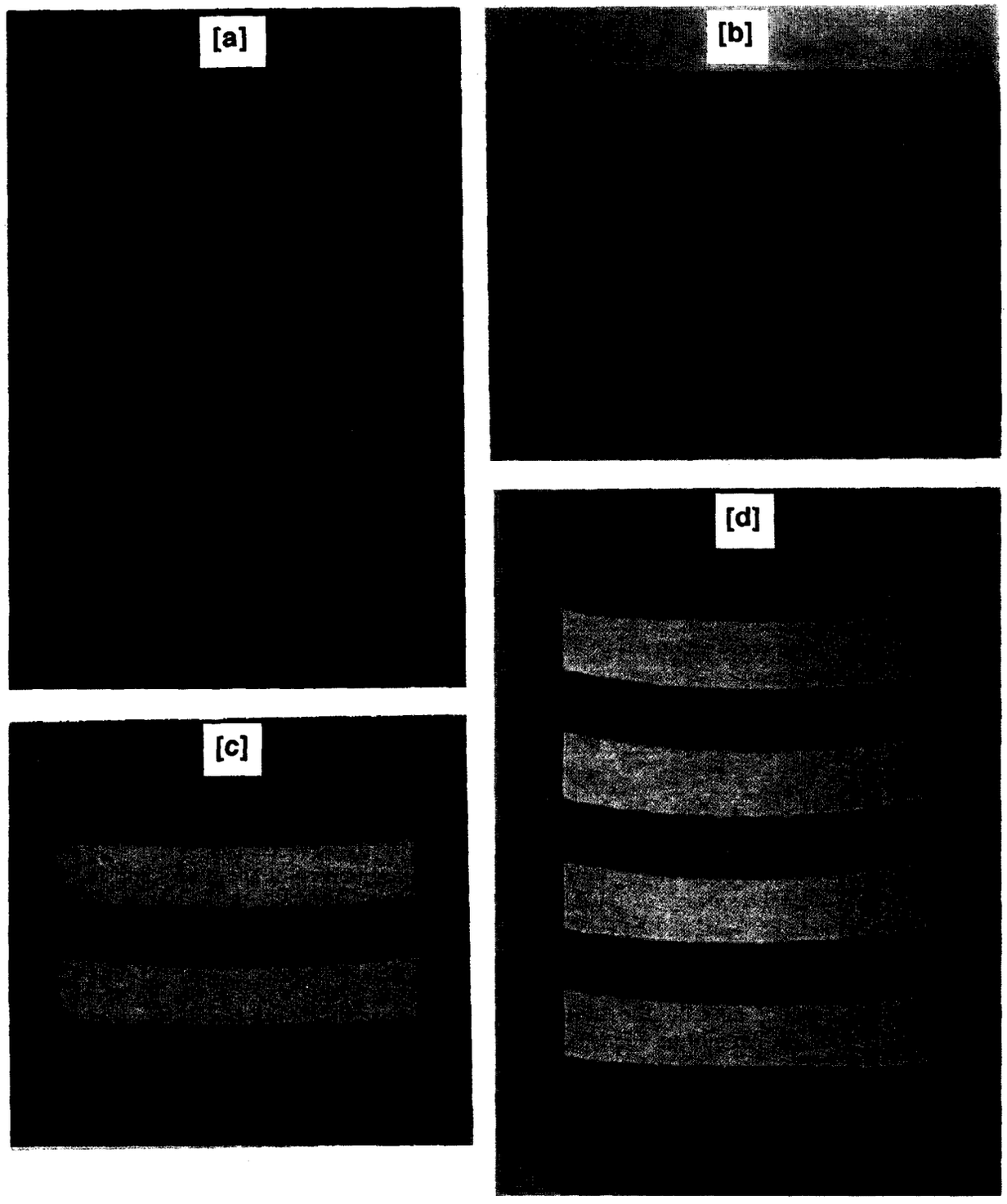

Fig. 7. Axial cross-sections of M/4·5/G/SD compacts, used for the density distribution calculations: (a) M/4·5/G/SD-[A]; (b) M/4·5/G/SD-[B]; (c) M/4·5/G/SD-[C]; and (d) M/4·5/G/SD-[D].

where P is the applied load, A is the projected area of the contact, h_p is the assumed depth of the residual plastic penetration at the load P and R is the radius of the spherical indenter. In order to determine the densities of the compact at selected points, a relationship between the density and the hardness was obtained by measuring the hardness of the relatively homogeneous compacts pressed at various compaction pressures.

The density at selected points on the surface of the compact was determined by indentation hardness measurements using the established relationship between the hardness and density, which was determined by using homogeneous thin compacts. Figure 11 shows these density values at selected points of the compact C (see Table 4). These density values were obtained from four separate hardness measurements. Although the hardness

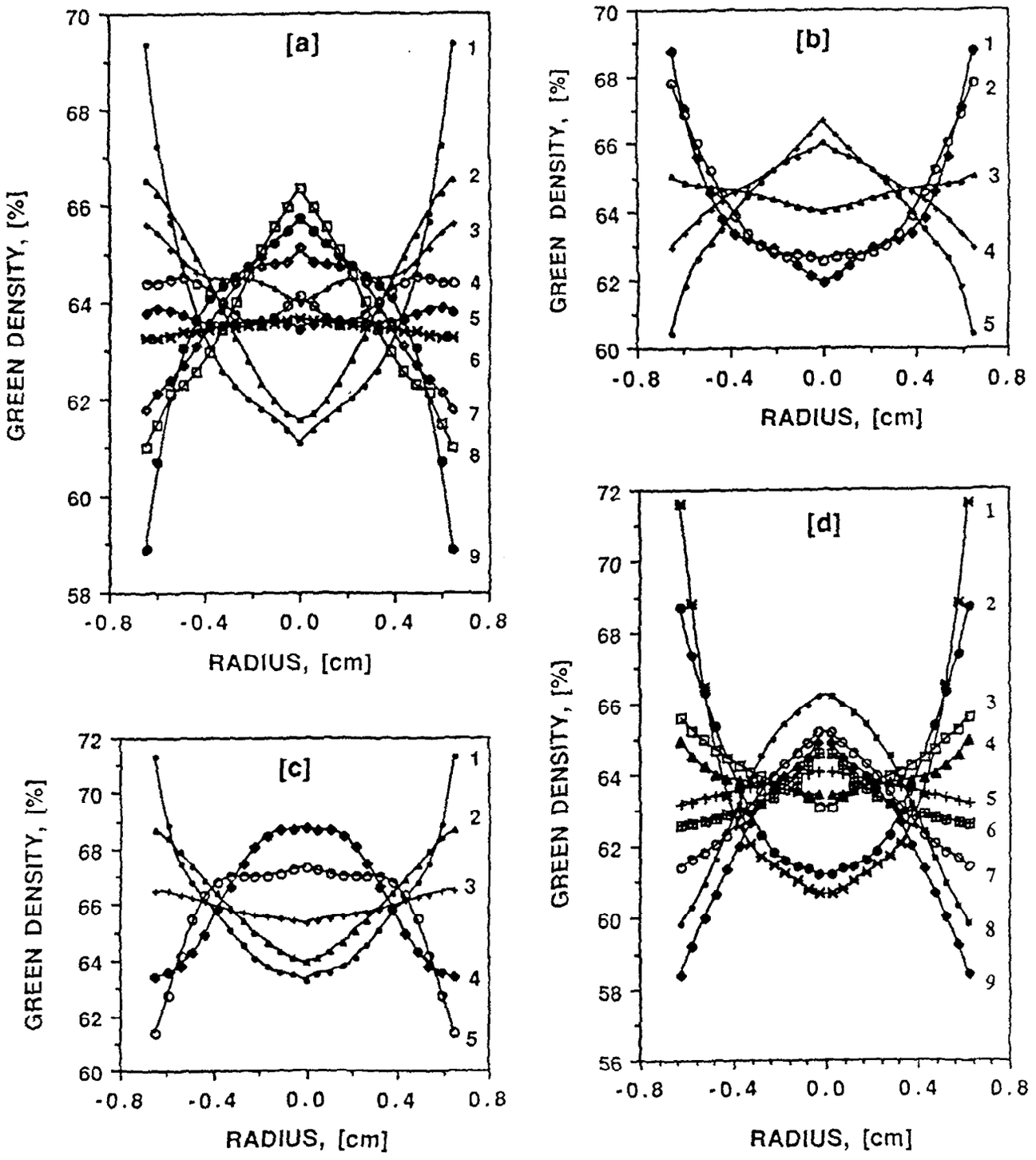

Fig. 8. Density distributions of the compacts: (a) M/4·5/G/SD-[A]; (b) M/4·5/G/SD-[B]; (c) M/4·5/G/SD-[C]; and (d) M/4·5/G/SD-[D]. The numbers (1, 2, 3 ...) represent the coloured layers.

Table 4. Properties of the compacts used for the density distribution calculations

Compact[a]	*Aspect ratio, H/D*[b]	*State of lubrication*[c]	*Compaction pressure (MPa)*[d]
M/4·5/G/SD-[A]	1·537	Lubricated	222
M/4·5/G/SD-[B]	0·846	Lubricated	222
M/4·5/G/SD-[C]	0·827	Lubricated	370
M/4·5/G/SD-[D]	1·552	Unlubricated	222

[a]For the properties of the compacts see Table 1.
[b]Aspect ratio of the compacts at the ultimate compaction pressure.
[c]The lubricated state was achieved by applying the zinc stearate powder to the die walls using a brush.
[d]Ultimate compaction pressure.

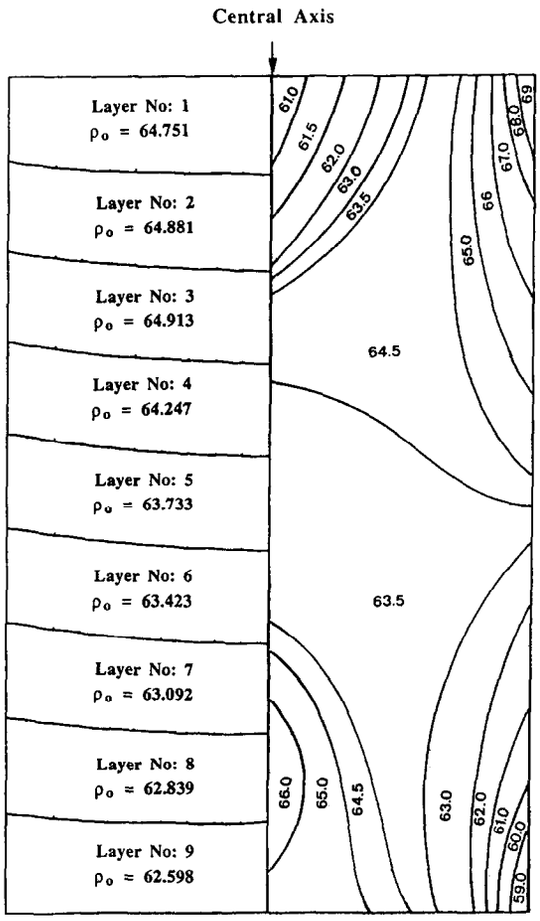

Fig. 9. Mean density of the layers together with the density distribution pattern for the compact M/4·5/G/SD-[A] (lubricated wall).

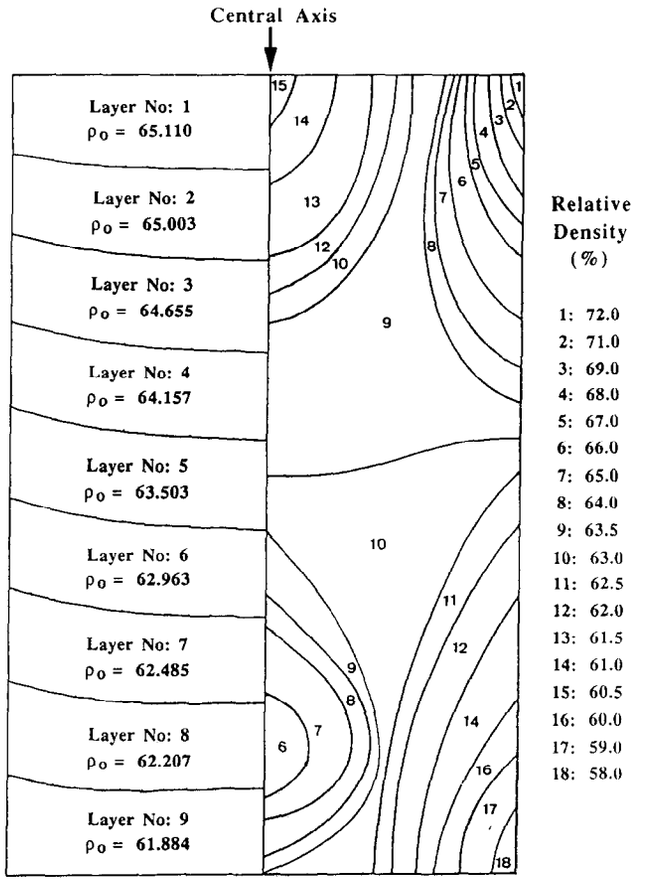

Fig. 10. Mean density of the layers together with the density distribution pattern for the compact M/4·5/G/SD-[D] (unlubricated wall).

measurements show a large scatter, it is quite clear that the hardness, or the green density, decreases towards the centre of the compact at the top of the compact and increases towards the centre of the compact at the bottom of the compact. These results are in general agreement with those obtained from the coloured layer technique described earlier.

3.4 First-order predictive model for density distributions

The compaction of a powder, constrained by a cylindrical geometry, was described by Janssen[14] using a first-order analysis which was subsequently modified by Walker.[15] The elementary form of the Janssen–Walker analysis (J–W analysis) assumes that no stress (and hence, in the current context, density) variations exist in planes orthogonal to the applied stress direction. According to the J–W analysis, the transmission ratio, as a function of the aspect ratio (H/D), is given by the following equation.[2,16]

$$\textit{Transmission ratio} = \frac{\bar{\sigma}_{yy}}{Q} = \exp\left(-C\frac{H}{D}\right) \qquad (12)$$

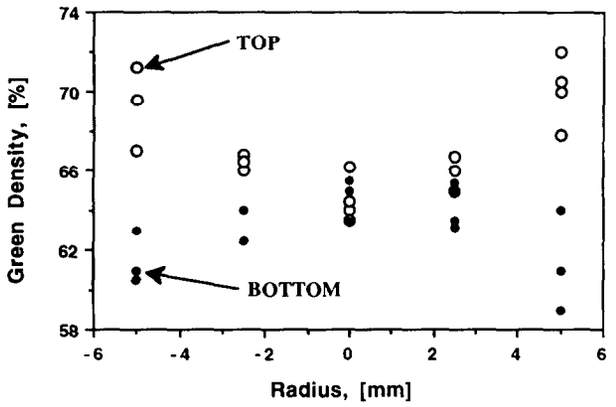

Fig. 11. Green density values at selected points for the top and the bottom surfaces of the compact M/4·5/G/SD-[C].

where $C = 4\ \mu K_w F$ (μ is the wall friction coefficient, K_w is a coefficient which depends on the equilibrium rheological state of the material and F is the distribution factor), $\bar{\sigma}_{yy}$ is the transmitted pressure, and Q is the applied pressure. At $y = 0$ ($H = 0$), at the top of the die, the mean stress is equal to the mean applied pressure (Q) and at $y = H$, at the bottom of the die, the mean stress is equal to the mean transmitted pressure. In order to calculate the mean stress as a function of the

height of the compact, the following equation may be used:

$$\bar{\sigma}(h) = Q \exp\left(-C\frac{h}{D}\right) \tag{13}$$

where h is the distance from the top surface of the compact.

Prediction of the density distribution along the height axis of the compact requires an interrelationship between the compaction pressure and density. It has been shown that, when the green density is plotted as a function of the logarithm of compaction pressure for an agglomerated powder, the compaction curve shows two or three distinct and rather linear regions.[1,17,18] The interrelationship between the compaction pressure and density, after the compaction yield pressure, may be accurately described in the form of the following simple empirical equation:

$$\rho = A + B\ln(\sigma) \tag{14}$$

Combining eqns (13) and (14) produces the following equation which will be adopted to predict the mean density distribution along the height axis of the compact:

$$\bar{\rho}(h) = A + B\ln(\bar{\sigma}(h))$$

$$\bar{\rho}(h) = A + B\ln Q - BC\frac{h}{D} \tag{15}$$

where $\bar{\rho}(h)$ is the mean density of the compact at the chosen height h of the compact and $\bar{\sigma}(h)$ is the corresponding mean stress level. Equation (15) is used later to predict the values of the mean density along the height axis of the compact using measured values of the quantities A, B and C.

3.4.1 Estimation of the constants A, B *and* C

Adopting eqn (12), the value of C is calculated from the slope of the plot of $\ln(\bar{\sigma}_{yy}/Q)$ versus H/D. This type of plot is illustrated in Figs 12(a) and (b) for the A/2·5/V/SD and M/4/G/SD alumina compacts, respectively.

In order to estimate the constants A and B, compacts with low aspect ratios (~0·15) were produced using various ultimate compaction pressures ranging from 74 to 740 MPa; essentially it was assumed that for these thin samples the transmission ratio was unity which was nearly the case. By the use of eqn (14), the constants A and B were calculated from the intercept and the slope of the plot, respectively (the green density versus the logarithm of the compaction pressure). The pressure value in eqn (14) is replaced with the effective average stress value, $\bar{\sigma}_{ea}$, which is obtained by integrating eqn (13) with respect to h (the height of the compact):

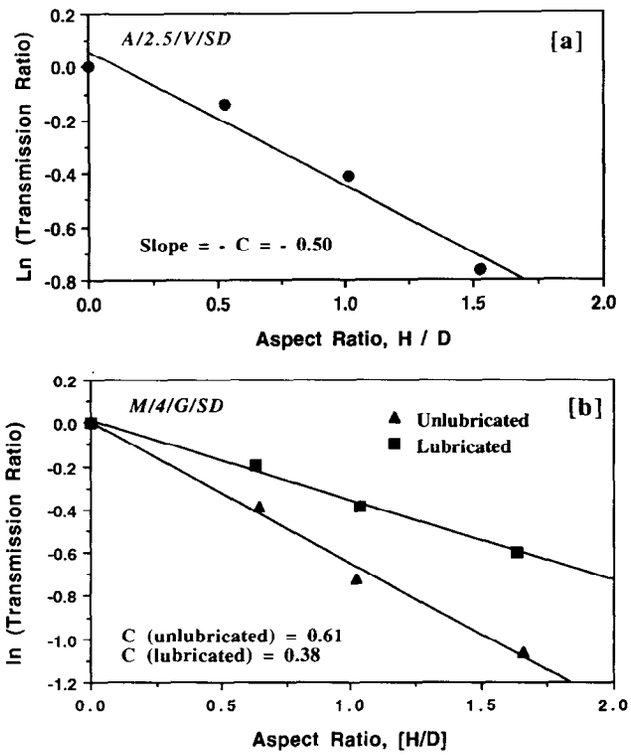

Fig. 12. Ln(transmission ratio) versus aspect ratio for (a) A/2·5/V/SD and (b) M/4/G/SD compacts.

$$\bar{\sigma}_{ea} = \frac{\int_0^{h_f} Q \exp\left(-C\frac{h}{D}\right)dh}{h_f} = Q\frac{\frac{D}{C}\left[1 - \exp\left(-C\frac{h_f}{D}\right)\right]}{h_f} \tag{16}$$

where h_f is the final height of the compact.

The relative green density versus the natural logarithm of the effective compaction pressure for the A/2·5/V/SD agglomerates is illustrated in Fig. 13. The values of the parameters A, B and C for the alumina agglomerates are given in Table 5.

It has already been shown that the sample aspect ratio strongly influences the final mean

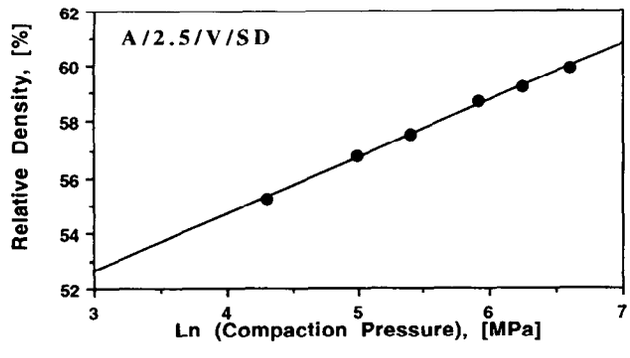

Fig. 13. Relative green density versus natural logarithm of the effective compaction pressure for the A/2·5/V/SD agglomerates.

Table 5. Values of A, B and C for the alumina compacts

Compact ID[a]	*Binder type & content (wt%)*[b]	*State of lubrication*[c]	A[d]	B[d]	C[e]
A/2·5/V/SD	2·45 PVA	Lubricated	46·74	2·01	0·50
M/4·5/G/SD	4·78 PEG	Lubricated	49·50	2·86	0·47
M/4/G/SD	4·12 PEG	Lubricated			0·38
M/4/G/SD	4·12 PEG	Unlubricated			0·61
A/2/G/D	2·4 PEG	Lubricated	51·70	1·30	0·34
A/2/G/W	2·4 PEG	Lubricated	52·33	1·24	0·32
A/2/G/H	2·4 PEG	Lubricated	52·07	1·25	0·33
A/4/G/W	4·7 PEG	Lubricated			0·35
A/2/V/D	2·4 PVA	Lubricated	47·75	1·89	0·37
A/2/V/W	2·4 PVA	Lubricated	50·55	1·56	0·34

[a]For the properties of the compacts see Table 1.
[b]PVA, poly(vinyl alcohol); PEG, poly(ethylene glycol).
[c]The lubrication state was achieved applying the zinc stearate powder to the die walls using a brush.
[d]Parameter in the empirical compaction equation [eqn (14)].
[e]Parameter in the J–W analysis [eqn (12)].

green density of these compacts. Therefore, a sufficient compaction equation should contain the aspect ratio as a parameter. Equation (15) may be integrated, with respect to the height of the compact, to provide a relationship between the mean green density $\bar{\rho}$ and the compact aspect ratio (h_f/D):

$$\bar{\rho} = \frac{\int_0^{h_f} \left(A + B\ln Q_a - BC\frac{h}{D} \right) dh}{h_f} = A + B\ln Q_a - \frac{1}{2}BC(h_f/D) \quad (17)$$

It has been noted previously that the experimental compaction curves consist of different stages, presumably corresponding to the different compaction mechanisms. Therefore, a single empirical equation cannot accurately describe the entire compaction process. Equation (17) may be used to predict the mean density of the compacts for a given compaction pressure range. The practical, or useful, compaction pressure will be higher than the second yield pressure (the joining pressure), which represents the termination stage of the closure of the interagglomerate pores. Table 6 shows the predicted [using eqn (17)] and measured mean green densities of the alumina compacts. Good agreement between the predicted results and the experimental results confirms the validity of eqn (17), which contains the three empirically measured parameters, A, B and C.

3.4.2 Comparison of experimental and predicted density distribution results

The predicted results and the experimentally measured average densities of the slabs from top to bottom of the compact for the compacts A (lubricated) and D (unlubricated) are illustrated in Figs 14(a) and (b), respectively. The predicted mean densities of both compacts decrease towards the bottom of the compact. However, in the case of compact A (lubricated), the experimentally measured density of the top slab is not the highest, rather it is the third slab from the top that has greatest density. Even though good agreement between the predicted and experimental results is obtained, the exact features of the density distribution along the height of the compact are not predicted. This first-order density distribution prediction is based on the J–W analysis, combined with the empirical interrelationship between the green density and the compaction pressure. The J–W analysis predicts that the transmitted pressure decreases uniformly as the distance from the pressure source increases. This is only the case if a loose powder bed of infinite extent is subjected to a static pressure. In the compaction process, the powder is confined in a die; as a result, the pressure is no longer transmitted uniformly but conforms to a characteristic stress pattern imposed by the die wall restraint. The analysis assumes the presence of no stress (and hence density) variations in planes orthogonal to the applied stress direction. As can be seen clearly from Fig. 9, there are density variations in the planes orthogonal to the applied stress direction. The disagreement between the predicted and experimental density distribution results, near the top of the compact, may be attributed to the inadequacy of the assumptions included in the J–W analysis. However, using this first-order density distribution analysis combined with the appropriate sintering simulations, the overall shape of the die pressed compacts may be reasonably predicted.[2]

Table 6. Predicted and measured mean green densities of the alumina compacts

Compact[a]	*Pressure (MPa)*[b]	*Aspect ratio*[c]	*State of lubrication*[d]	ρ_o(%) *experimental*[e]	ρ_p(%) *predicted*[f]	% *Error*[g]
M/4·5/G/SD	222	1·536	Lubricated	63·92	63·92	0·00
M/4·5/G/SD	222	1·520	Lubricated	63·82	63·93	0·17
M/4·5/G/SD	222	1·540	Lubricated	64·05	63·92	0·20
M/4·5/G/SD	222	0·845	Lubricated	64·52	64·38	0·22
M/4·5/G/SD	222	0·849	Lubricated	64·44	64·38	0·09
M/4·5/G/SD	222	0·852	Lubricated	64·39	64·38	0·02
M/4·5/G/SD	222	0·504	Lubricated	64·53	64·60	0·11
M/4·5/G/SD	222	0·507	Lubricated	64·52	64·60	0·12
M/4·5/G/SD	370	0·826	Lubricated	65·96	65·85	0·17
M/4·5/G/SD	370	0·829	Lubricated	65·98	65·85	0·20
M/4·5/G/SD	74	0·24	Lubricated	61·60	61·65	0·08
M/4·5/G/SD	74	0·48	Lubricated	61·48	61·47	0·08
M/4·5/G/SD	74	0·72	Lubricated	61·38	61·31	0·11
M/4·5/G/SD	74	0·96	Lubricated	61·27	61·16	0·18
M/4·5/G/SD	74	1·19	Lubricated	61·15	61·00	0·08
M/4·5/G/SD	74	0·24	Unlubricated	61·46	61·56	0·16
M/4·5/G/SD	74	0·49	Unlubricated	61·28	61·31	0·05
M/4·5/G/SD	74	0·73	Unlubricated	61·11	61·07	0·07
M/4·5/G/SD	74	0·96	Unlubricated	60·96	60·84	0·20
M/4·5/G/SD	74	1·20	Unlubricated	60·69	60·60	0·15
M/4·5/G/SD	40	0·74	Lubricated	59·75	59·55	0·33
M/4·5/G/SD	74	0·73	Lubricated	61·21	61·31	0·16
M/4·5/G/SD	148	0·70	Lubricated	63·19	63·32	0·21
M/4·5/G/SD	296	0·68	Lubricated	65·18	65·31	0·20
M/4·5/G/SD	518	0·66	Lubricated	67·01	66·93	0·12
M/4·5/G/SD	740	0·65	Lubricated	68·16	67·98	0·26
M/4·5/G/SD	40	0·74	Unlubricated	59·44	59·31	0·12
M/4·5/G/SD	148	0·70	Unlubricated	62·85	63·09	0·38
M/4·5/G/SD	296	0·69	Unlubricated	64·97	65·07	0·15
M/4·5/G/SD	518	0·66	Unlubricated	66·78	66·71	0·10
A/2·5/V/SD	145	1·53	Lubricated	55·88	55·98	0·18
A/2·5/V/SD	145	1·01	Lubricated	56·18	56·24	0·10
A/2·5/V/SD	145	0·52	Lubricated	56·33	56·48	0·27
A/2·5/V/SD	74	~1·0	Lubricated	54·89	54·85	0·07
A/2·5/V/SD	148	~1·0	Lubricated	56·18	56·23	0·09
A/2·5/V/SD	290	~1·0	Lubricated	57·47	57·58	0·19

[a]For the properties of the compacts see Table 1.
[b]Ultimate compaction pressure.
[c]Aspect ratio of the compacts at the ultimate compaction pressure.
[d]The lubrication state was achieved by application of the zinc stearate powder to the die walls using a brush.
[e]ρ_0 = the measured green density.
[f]ρ_p the predicted green density using eqn (17).
[g]%Error = $(|\rho_o - \rho_p|/\rho_0) \times 100$.

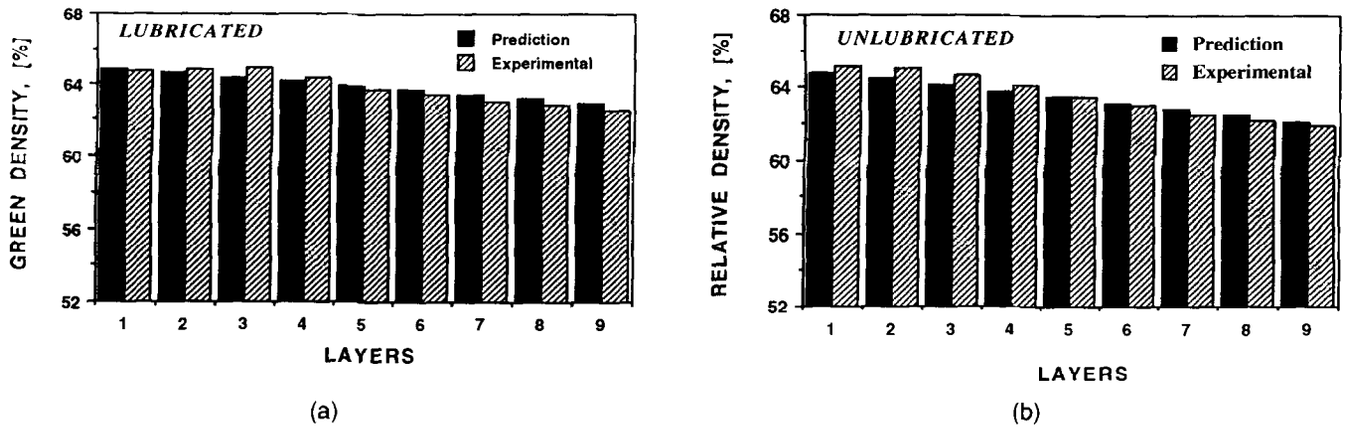

Fig. 14. Predicted results and experimentally measured average densities of the discrete slabs for (a) M/4·5/G/SD-[A] (lubricated wall) and (b) M/4·5/G/SD-[D] (unlubricated wall).

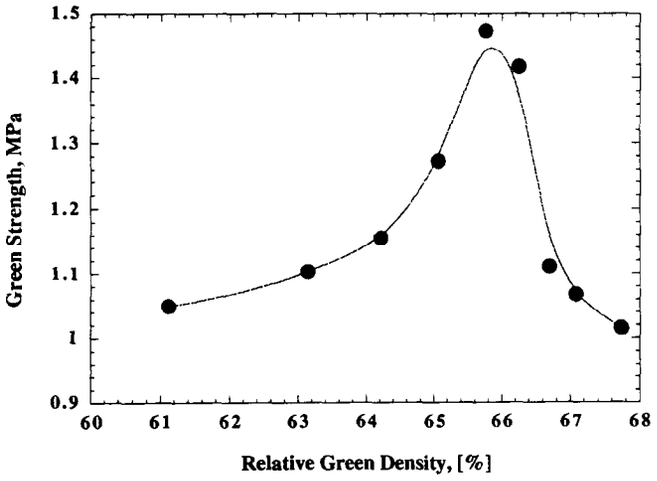

Fig. 15. Green strength of the M/4·5/G/SD alumina compacts as a function of green density.

3.5 Relationship between green strength and green density

The present green specimens were freed of the constraints of the die by the process of ejection, using the same punch that provided the initial densification. The ejection process may provide an additional compaction but the most important factor is that it allows the release of the stored strains in the green body in a progressive way.

Figure 15 shows the variation of the green strength as a function of the mean ejected compact density. Initially, the strength increases more than exponentially with the green density. At a certain critical density, the strength begins to decline. This observation may be explained in general terms as follows. The green compacts contain pores which may act as the strength-limiting defects. The fracture strength of the materials depends upon the crack length a, and the radius of curvature at the tip c,[19] of the voids within the green. With the increasing density of the green compacts, the size of the pores in the green body will be reduced and thus the magnitude of the crack length and the radius of the curvature will be strongly affected; both will decrease. The strength will scale roughly with the ratio $(c/a)^{0.5}$. The decrease of the green strength beyond the critical density (or compaction pressure) is due to the formation of large laminar cracks within the green compact during the ejection process which weaken the coherence of the body. The effect is marked and, at the highest compaction levels, the strengths of the green bodies are lower than those of the very lightly compacted material.

4 Summary and Conclusions

The applied and transmitted pressures have been recorded simultaneously during the compaction process for a simple compaction geometry. It has been found that the transmitted pressure decreases as the aspect ratio of the compacts increases. The state of wall lubrication strongly affects the transmission ratio; that is, the transmission ratio is increased with the application of an effective lubricant on the die wall.

The density distributions in the alumina compacts have been determined experimentally, using the coloured layer technique and indirectly using hardness measurements. The results obtained from these two experiments are in good agreement. The densest parts of the compacts, pressed uniaxially from the top, are at the outer circumference at the top and the least dense parts are at the outer circumference at the bottom. The density near the surface of the compacts decreases with height from the top to the bottom of the compact. The density difference between the densest and the least dense parts of the compacts increases with increasing aspect ratio.

The density distributions in the alumina compacts have also been estimated using a first-order predictive model. According to the model, the mean density along the height of the compact decreases linearly with height from the top to the bottom of the compact. The predictions are nearly in accord with experiment.

Measurements of the strength of these green bodies indicate that there is an optimal compaction pressure and density for the production of the strongest greens. Although the green density increases as the compaction pressure increases beyond a certain level, so does the stored elastic stresses which are relaxed upon ejection. These stored stresses induced internal cracks in the green bodies which create sources of weakness and induce defects which precipitate fracture.

Acknowledgement

The authors would like to acknowledge the financial support of British Nuclear Fuels plc for the ceramic processing programme in the Particle Technology Group at Imperial College.

References

1. Briscoe, B. J. & Özkan, N., Compaction behaviour of agglomerated ceramic powders. *Powder Technol.*, (in press).
2. Özkan, N. & Briscoe, B. J., Prediction of overall shape of sintered alumina compacts. *J. Eur. Ceram. Soc.*, **14** (1994) 143.
3. Marion, R. H. & Johnson, J. K., A parametric study of diametral compression test for ceramics. *Am. Ceram. Soc. Bull.*, **56**[11] (1977) 998.

4. Balshin, M. Y., The theory of the process of pressing. *Vestnik Metalloprimishlennosli*, **18** (1938) 124.
5. Train, D., An investigation into the compaction of powders. *J. Pharm. London*, **8** (1956) 745.
6. Kamm, R., Steinberg, M. & Wulff, J., Plastic deformation in metal-powder compacts. *Trans. AIME*, **171** (1947) 439.
7. Aketa, Y., Tanaka, Y. & Tsuwa, H., Studies on compacting of metal powder. *Technology Reports of Osaka University*, **15** (1965) 81.
8. van Groenou, A. B. & Knaapen, A. C., Density variations in die-compacted powders. *Sci. Ceram.*, **10** (1980) 93.
9. Charlton, B. & Newton, J. M., Application of gamma-ray attenuation to the determination of density distributions within compacted powders. *Powder Technol.*, **41** (1985) 123.
10. Kuczynski, G. C. & Zaplatynskyj, I., Density distribution in metal powder compacts. *Trans. AIME*, **8** (1956) 215.
11. Kandeil, A. & de Malherbe, M. C., The use of hardness in the study of compaction behaviour and die loading. *Powder Technol.*, **17** (1977) 253.
12. Özkan, N., Compaction and sintering of ceramic powders. Ph.D. Thesis, Imperial College, London, 1994.
13. Adams, R. A., *Single Variable Calculus*. Addison Wesley Publishers, London, 1990.
14. Janssen, H. A., Versuche Uber Getreiddruck in Silozellen. *Z. Ver. Deutsch. Ing.*, **29** (1895) 1045.
15. Walker, D. M., An approximate theory for pressures and arching in hoppers. *Chem. Eng. Sci.*, **21** (1966) 275.
16. Briscoe, B. J., Fernando, M. S. D. & Smith, A. C., The role of interface friction in the compaction of maize. In *Tribology in Particulate Technology*, eds. B. J. Briscoe & M. J. Adams. IOP Publishing, London, 1987, p. 220.
17. Lukasiewicz, S. J. & Reed, J. S., Characterisation and compaction response of spray-dried agglomerates. *Am. Ceram. Soc. Bull.*, **9** (1978) 798.
18. Dimilia, R. A. & Reed, J. S., Dependence of compaction on the glass transition temperature of the binder phase. *Am. Ceram. Soc. Bull.*, **62**[4] (1983) 484.
19. Knott, J. F., *Fundamentals of Fracture Mechanics*. Butterworths, London, 1973.